HOSTED BY

ELSEVIER

Available online at www.sciencedirect.com

ScienceDirect

Journal of Magnesium and Alloys 4 (2016) 83–88
www.elsevier.com/journals/journal-of-magnesium-and-alloys/2213-9567

Full Length Article

The effect of LPSO on the deformation mechanism of Mg–Gd–Y–Zn–Zr magnesium alloy

Jianbo Shao, Zhiyong Chen *, Tao Chen, Zhang Hu, Xiaojie Zhou, Chuming Liu

School of Materials Science and Engineering, Central South University, Changsha 410083, China

Received 29 October 2015; revised 2 March 2016; accepted 15 March 2016

Available online 20 April 2016

Abstract

The tensile deformation behavior and corresponding microstructure evolution of the Mg-4.7Gd-3.4Y-1.2Zn-0.5Zr (at. %) magnesium alloy with long period stacking structure (LPSO) are studied by electron backscatter diffraction (EBSD) and slip lines methods. The results show that less and very small size of twins is observed in the grains with high value of Schmid factor for twinning, which indicates that the growth of the {10–12} twinning deformation is prevented by the LPSO phase. The prismatic lines present in grains of which the prismatic slip Schmid factor is above 0.4. The favorable orientation and LPSO phase synergistically promote the activation of prismatic slip. The inhomogeneous rotation of the grains during deformation is the reason for the microcrack at grain boundary.

Keywords: Rare earth magnesium alloys; LPSO; Deformation mechanism; Crystal orientation

1. Introduction

Magnesium and its alloys have received more and more attention from the engineering applications owing to the low density, high specific strength and excellent damping capacity [1–3]. However, the poor mechanical properties limited its further application in automotive and electronics industries as well as modern aerospace. Therefore, great efforts have been devoted to improve the strength and ductility of magnesium alloys [4–6]. The $Mg_{97}Zn_1Y_2$ (at. %) alloy that produced by rapidly solidified powder metallurgy processing exhibited excellent mechanical properties with a tensile yield strength of ~600 MPa and elongation of ~5% at room temperature and the excellent properties were attributed to the fine grain and LPSO phase [4]. Recently, the sheet produced by rolling and ageing treatment exhibited excellent properties with ultimate tensile strength of 517 MPa, 0.2% proof stress of 426 MPa and elongation to failure of 4.5% [5]. In addition, the formation of LPSO phase in the rare earth magnesium alloys was found to maintain the stability of the yield and ultimate strength at elevated temperature, which may broaden the applications of magnesium alloys as structure materials at elevated temperature [6].

With the classification and structure of LPSO phase including 10H, 14H, 18R and 24R types were acknowledged gradually by previous studies [7–12], the effect of LPSO phase on the deformation mechanism of magnesium alloys becomes a problem that should be solved urgently. M. Matsuda found that the existence of LPSO phase could increase the critical resolved shear stress (CRSS) of basal plane and promote the activation of non-basal plane slip [13] and this conclusion was also approved by the first principle calculations [14]. However, K. Hagihara thought that the (0001) < 11–20 > basal slip and deformation kinks were the dominant deformation mode in the compression deformation for both 14H-typed and 18R-typed LPSO phase and the CRSS of basal slip was estimated to be 10–30 MPa [15,16]. Recently, researchers found that the deformation mode of LPSO is basal <a > slip or kink-banding, while magnesium matrix deformed by basal <a > slip and pyramidal <c + a > slip [17]. Furthermore, the LPSO phase was seen to behave elastically, even after the macroscopic yield stress and into the stress plateau and the existence of LPSO may inhibit or delay twining deformation [18]. In fact, crystal orientation has great influence on the activation of slip system and twinning deformation. Therefore, it is necessary to take the grain orientation into account when studying the effect of LPSO phase on

* Corresponding author. School of Materials Science and Engineering, Central South University, Changsha 410083, China. Tel.: +86 139749260192; fax: 0731-88876692.

E-mail address: czysh@netease.com (Z. Chen).

http://dx.doi.org/10.1016/j.jma.2016.03.001

deformation mechanism. In this study, initial crystal orientation of grains are obtained by EBSD and the activation of twinning deformation and corresponding Schmid factor (SF) is studied by EBSD. In addition, the shape and surface morphology of grains are observed by SEM and slip lines method are also applied to study the activation of slip systems.

2. Experimental procedure

The schematic illustration of the uniaxial tensile sample is given in Fig. 1. The tensile samples were machined from an extruded Mg-4.7Gd-3.4Y-1.2Zn-0.5Zr (wt.%) magnesium alloy bar prepared by hot extrusion at 400 °C with a reduction ratio of 10.

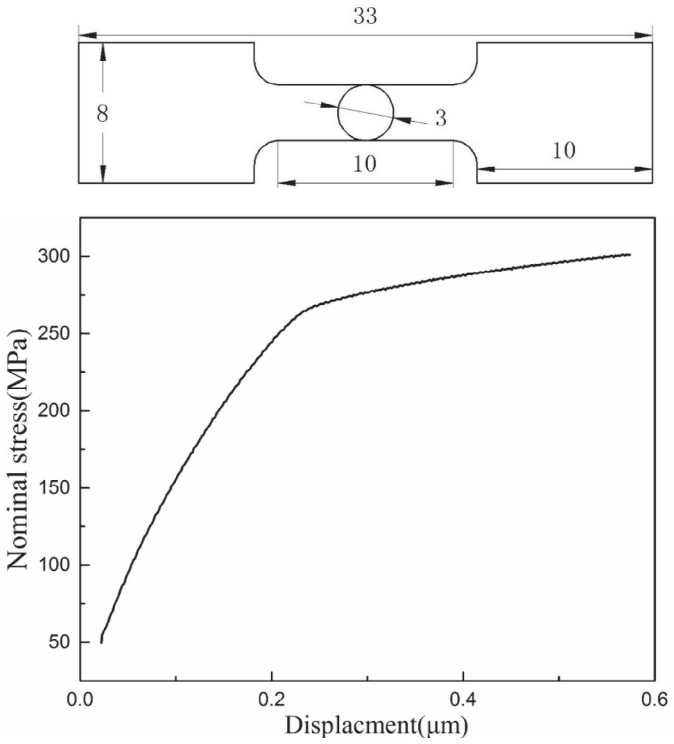

Fig. 1. Tensile specimen with flat faces inside circle and for EBSD measurements and plastic deformation (~3.5%) of the sample for deformation mechanism study.

The texture variation of the tensile sample before and after tensile deformation was measured by EBSD in the same region. Uniaxial tensile tests were conducted at room temperature with 1 mm/min tensile rate. The plastic deformation for tensile testing is closed to 3.5% and the nominal stress-displacement curve is shown in Fig. 1. The region for the EBSD measurements was prepared by electro polishing in the RD × ND plane, indicated by a circle in the Fig. 1. Specimens for EBSD and TEM measurement were prepared by mechanical polishing and electro polishing using a solution of 60% methanol, 35% n-butyl alcohol and 5% perchloric acid on Automatic Twin-Jet Electro polishing device at 30 V and −30 °C. The texture measurement was carried out by a HELIOSN NANOLAB 600i SEM equipped with HKL Channel 5.0 software and the scanning step is 0.6 μm. TEM images and corresponding selected area electron diffraction (SAED) patterns were obtained using an FEI Titan G2 60–300 electron microscope equipped with a field emission gun operating at 200 KeV. The region with slips was observed by scanning electron microscopy (SEM).

3. Results and discussion

The microstructure showing in Fig. 2a indicates that the Mg-4.7Gd-3.4Y-1.2Zn-0.5Zr alloys contains amount of intermetallic phases inside grain with different contrast comparing with magnesium matrix. The bright field TEM image and the electron diffraction patterns recorded along <11–20 > Mg direction in Fig. 2b confirm that these intermetallic phases are 14H-LPSO for the existence of thirteen additional spots between transmission spot and (0002) α spot (inset in Fig. 2b).

Fig. 3 shows inverse pole figure (IPF) maps of the tensile sample before and after deformation. Colors of grains in maps represent the crystal orientation with respect to the sample coordinate system. In the Fig. 3a, most of the grains are of blue and green color which indicates that a large number of grains *a*-axis is parallel to the transverse direction (TD) of extruded sheet. This

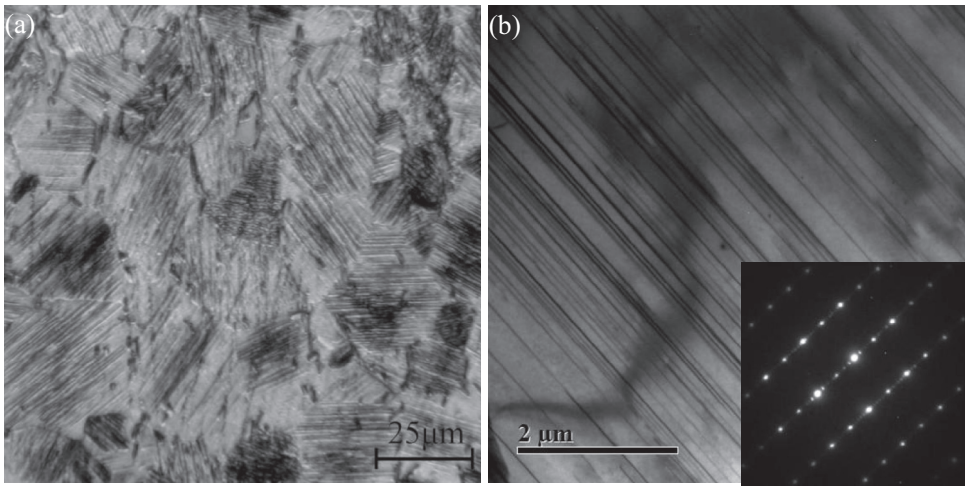

Fig. 2. (a) Optical micrograph of extruded Mg-4.7Gd-3.4Y-1.2Zn-0.5Zr (at. %) magnesium alloy; (b) Bright-field TEM micrograph of LPSO phase in the view of <11–20> $_{Mg}$ direction and the SAED pattern of the LPSO is shown in the insert to (b).

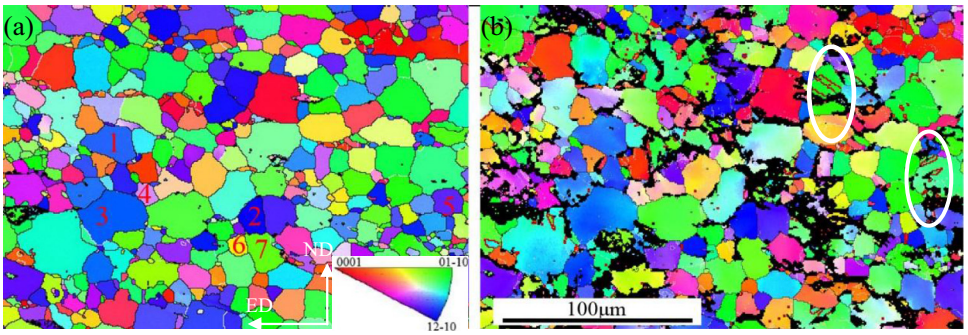

Fig. 3. EBSD inverse pole figure map of tensile sample: (a) before tensile deformation; (b) after tensile deformation.

texture characteristic of c-axis parallel to ED was also reported in other studies [19]. Compared with grains orientation before tensile test, the distribution of orientation in some grains is no longer homogeneous as shown in Fig. 3b. In addition, it is important to note that the black regions are obviously increased and the black regions are mainly located at grain boundary. The stress concentration at grain boundary for the serious plastic deformation may be the reason for the failed measurement by EBSD. Besides, small amount of deformation bands occur in the deformation process as illustrated with white oval in Fig. 3b. Crystallographic analysis confirms that the deformation bands are {10–12} extension twin (the red lines indicated the {10–12} twinning boundary). This type of twinning can cause a rotation of basal plane of an angle of about 86°.

Fig. 4 illustrates the texture characteristic of the sample before and after tensile deformation. As shown in Fig. 4a, the majority of grains *c*-axis is parallel to the extrusion direction (ED) or perpendicular to the normal direction (ND). After deformation, the variation of texture characteristic is not very obvious. The extension of contour line at a value of 4 in ND and shrinkage in the ED may be caused by the slight adjustment of some grains *c*-axis. The adjustment of grain c-axis can be

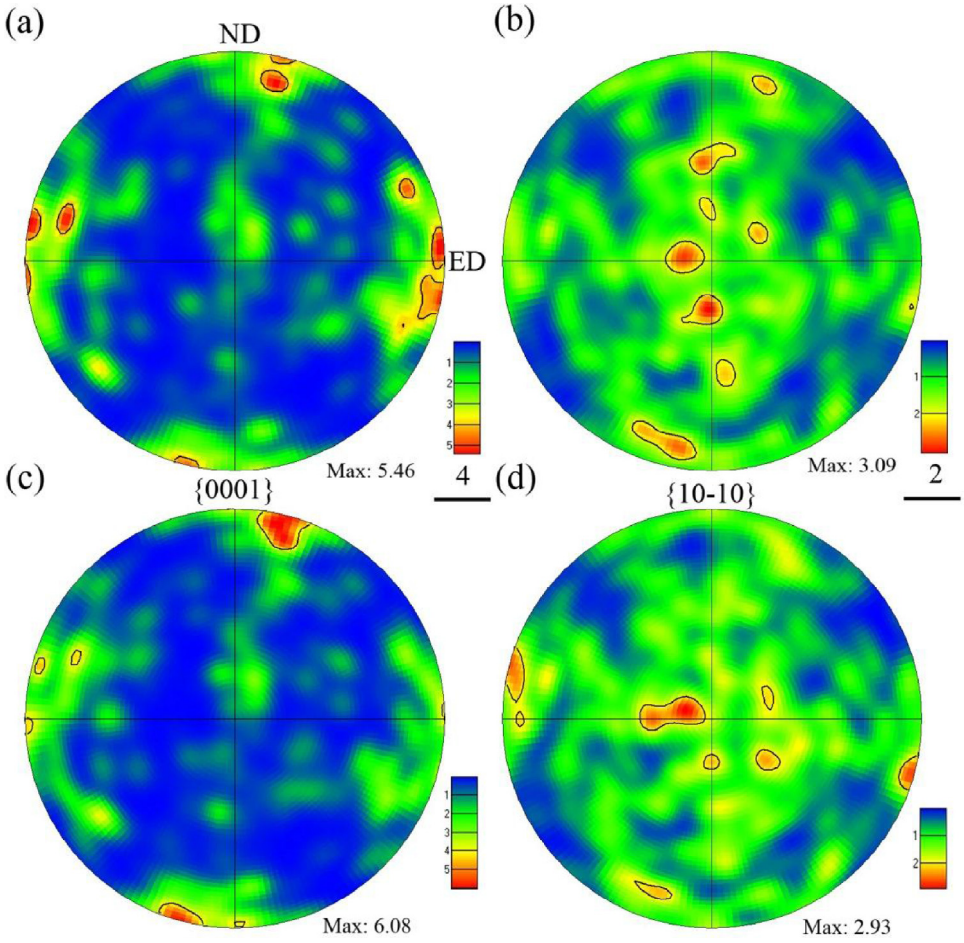

Fig. 4. The {0001} and {10-10} pole figure of tensile sample: (a) and (b) before deformation; (c) and (d) after deformation.

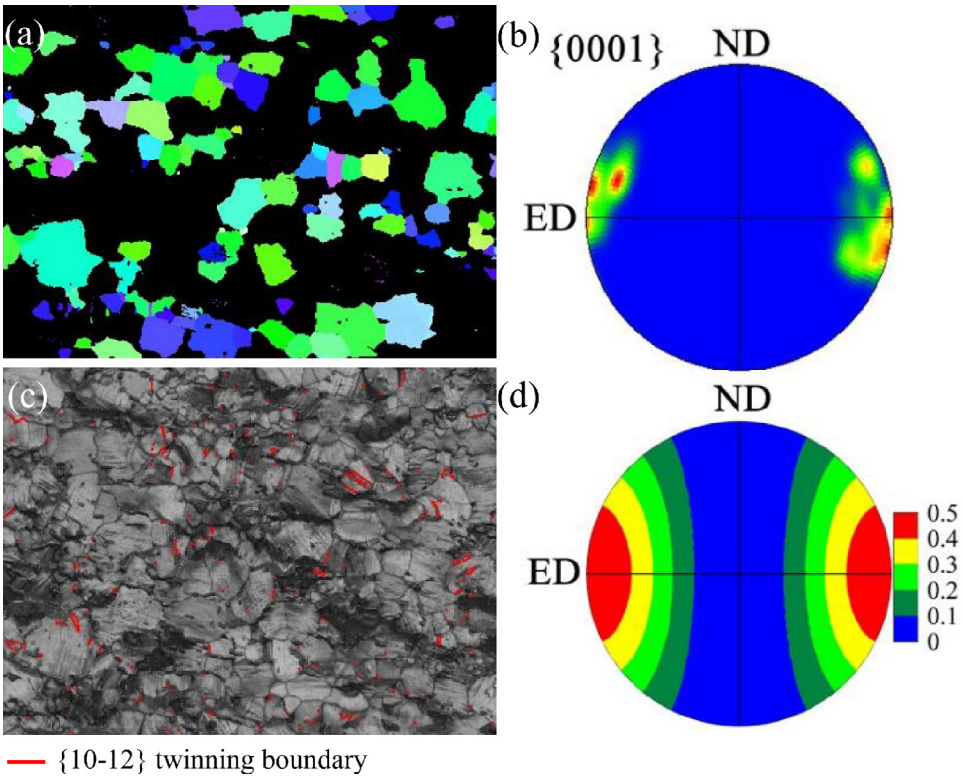

Fig. 5. (a) The IPF map of grins in the favorable orientation for twinning; (b) corresponding PF maps of the grains in (a); (c) the distribution of {10–12} twinning boundary indicated by red lines; (d) the distribution of SF for twinning in {0001} PF when loading along ED.

explained by the following two aspects. On one hand, the basal plane will rotate to parallel to loading direction for activation of basal plane during the tensile deformation [20]. On the other hand, twinning deformation can be activated easily in the grains whose c-axis parallel to tensile direction and the basal plane of matrix will be rotated with angle of 86°. The vast of activation of twinning deformation will cause great texture changes [20]. Similarly, the inapparent changes in texture can also be explained by the less numbers of twins.

Considering the effect of crystal orientation on twinning deformation, the grains in the favorable orientation for twinning (the Schmid factor above 0.4) is picked out according to the distribution of SF for {10–12} extension twinning in Fig. 5d. The IPF of the selected grains are shown in Fig. 5a. In addition, the twinning boundary marked with red line is also exhibited in Fig. 5c. Comparing Fig. 5a and c, it is interesting that only few and small twin boundaries can be observed, which means that the twinning deformation is prevented even in the grains with high twinning SF. Furthermore, the twin boundaries are mainly found around grain boundary and the twins moving across the whole grain are difficult to be observed. The above phenomenon implies that it is the growth process of deformation twins that is prevented instead of the nucleation process. The inhibition of twinning deformation in these favorable grains may be attributed to the existence of LPSO phase. Intragranular thin-platelet LPSO phases almost occupied the whole grain which may be a barrier for the growth of twins. Previous study found that the inhibition of LPSO phase for twinning is largely dependent on the size of LPSO phase [21]. The thickness of lamellar LPSO phase below 5nm could take place twinning deformation with matrix while twin have to bypasses the 12-nm-thick LPSO plate. It implies that twin can formation and propagation in the region with none LPSO phase or thin LPSO phase but it is inhibited by the LPSO with larger size. The mechanism that LPSO phase hinder twinning deformation is still not clear. K. Hagihara thought that the changes in the atomic arrangement on the pyramidal planes and the peculiar segregation of Y and Zn atoms on the specific layers could hinder the formation of {10–12} twin in Mg-LPSO alloys [15].

In general, magnesium alloy's plastic deformation at ambient temperature is considered to be dominated by basal slip or twinning. Obviously, twinning deformation is inhibited by LPSO phase. Hence, basal slip may play the dominant role in plastic deformation. However, considering the inhibition of LPSO phase to basal slip as mentation in the introduction, non-basal slip may be activated in those grains with high SF for prismatic slip. Therefore, the activation of non-basal slip is studied by slip line methods.

Fig. 6 presents several examples of non-basal slip lines indicated by white arrows. Compared with the 3D crystal, slip lines are mainly parallel to the prismatic plane, which indicated the occurrence of prismatic slip during testing. The number of slip lines in grains marked with numbers 1 and 3–5 is more than that in grain marked with 2, indicating that the higher of SF for prismatic slip may promote the movement of dislocations on prismatic plane (the SF of former is ranging from 0.4 to 0.46

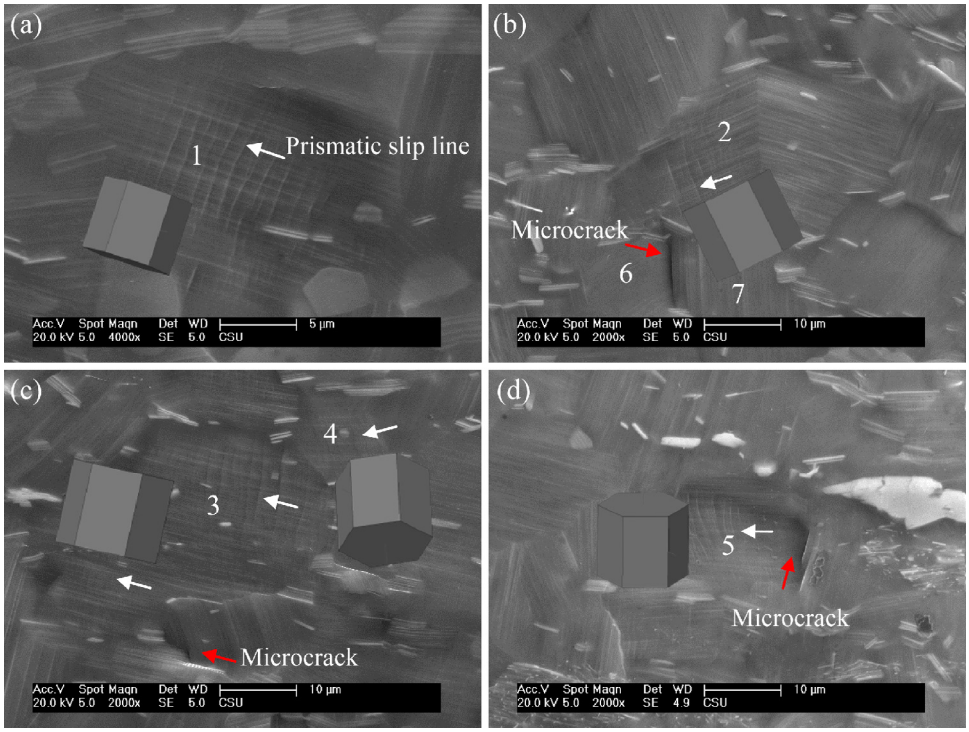

Fig. 6. Examples of identification of activated non-basal slip.

while the latter is 0.35). Datta et al. found that prismatic slip was preferred in a 6*l* structure (ABACAB) and inhibited in 2*l* (AB) structure and the authors confirmed that an increase in stacking periodicity can indeed promote activation of non-basal slip [14]. On the base of this point, the 14H LPSO exhibited exhibit longer stacking periodicity. Therefore, the activation of non-basal slip may be promoted synergistically by LPSO phase inside grains and favorable orientation for prismatic slip.

In addition, surface relief is observed after deformation which may be caused by the grains rotation with respect to the surrounding grains. The grain rotation not only can lower the total grain boundary energy and relax the stress concentration efficiently but also adjust the crystallographic orientations to the favorable orientation for further plastic deformation [22]. However, with the occurrence of grain rotation, some microcrack nucleation at grain boundary are also observed, as indicated by red arrows in Fig. 6. As shown in Fig. 6b, the grain rotation causes a pit formation in the right region of grain 6. By comparing the crystal orientation around that crack, the microcrack may be explained by the inconsistent grain rotation around the crack. The variation of the orientation in grain 6 and grain 7 is shown as inverse pole figures in Fig. 7b, which

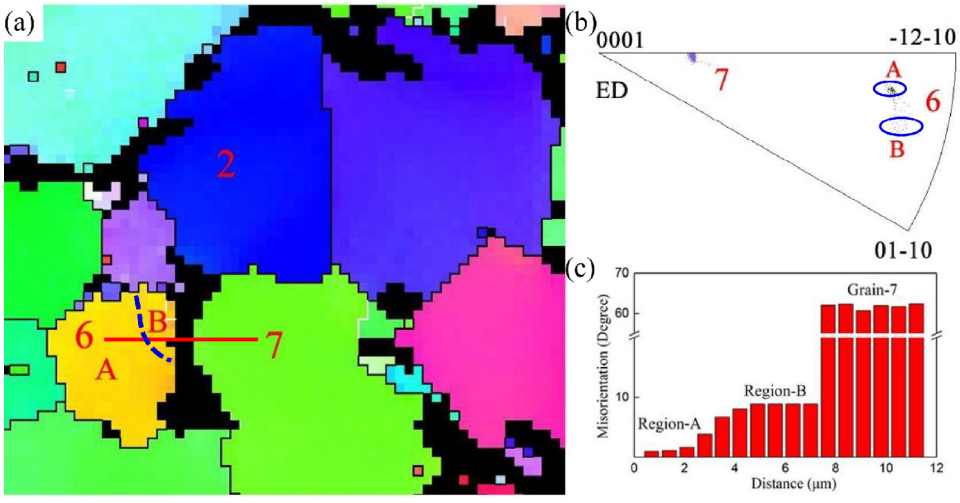

Fig. 7. The crystal rotation of the grins adjoin to the microcrack: (a) IPF map of the grains nearby microcrack (the region labeled as A and B for the different crystal orientation); (b) the changes of crystal orientation of grain 6 and grain 7 in IPF; (c) the point to origin misorientation angle along the red line.

represent the position of the tensile axis in the reciprocal space of the grains. The crystal orientation of regions A and B in grain 6 is labeled as A and B. It is easy to find that the crystal orientation of region B takes place great changes compared to region A and this grain rotation is limited to location region instead of the whole grain. Compared to grain 6, grain 7 exhibits inconspicuous variation. The misorientation evolution along the red line also indicated that the grain 6 exhibits more intense changes of crystal orientation than grain 7. These inconsistent changes of crystal orientation are the reason for the failed connection of grain boundary and finally cause the formation of microcrack and the microcrack will be further expended under the external load.

Considering the inhibition of twin deformation and the activation of non-basal slip in the Mg-LPSO alloy, the Mg-LPSO alloy may be a good candidate for the further improvement of mechanical properties of magnesium alloys. Firstly, the lack of twinning boundary reduces the nucleation sits of cracks. Somekawa found that the crack could propagate along the twin boundary and prevention of the formation of deformation twins was considered as an efficient methods to improve the fracture toughness [23]. In addition, the activation of non-basal slip promotes the more homogeneous plastic deformation of grains and reduces the concentration of stress. Furthermore, the kink deformation in Mg-LPSO alloys reported by other researchers can provide more pathway for plastic deformation and the kinking LPSO phase can strengthen the Mg alloys [24].

4. Summary

The texture evolution and the effect of LPSO phase on the deformation mode of Mg-4.7Gd-3.4Y-1.2Zn-0.5Zr magnesium alloy during uniaxial tensile deformation are studied and the main conclusions are presented as follows. The initial texture of Mg-4.7Gd-3.4Y-1.2Zn-0.5Zr magnesium alloys indicated a part of grains *c*-axis is parallel to the tensile direction and these grains are in the favorable orientation for {10–12} extension twinning. However, less and small size twins in these grains with high SF for twinning indicate that the {10–12} twinning is prevented by LPSO phase. The non-basal slip is activated in some grains by observing the slip line after deformation. The surface relief and microcrack at grain boundary are observed after deformation, which is caused by the rotation of grains with respect to each other.

Acknowledgements

The authors would like to thank Key Project of Chinese National Programs for Fundamental Research and Development (973 program), National Natural Science Foundation of China (NSFC) through project nos. 2013CB632202 and 51574291 respectively and the outstanding graduate project of Advanced Non-ferrous Metal Structural Materials and Manufacturing Collaborative Innovation Center.

References

[1] B.L. Mordike, T. Ebert, Mater. Sci. Eng. A 302 (2001) 37–45.
[2] S.R. Agnew, Ö. Duygulu, Int. J. Plast. 21 (2005) 1161–1193.
[3] M. Yamasaki, K. Hashimoto, K. Hagihara, Y. Kawamura, Acta Mater. 59 (2011) 3646–3658.
[4] K. Hagihara, A. Kinoshita, Y. Sugino, M. Yamasaki, Y. Kawamura, H.Y. Yasuda, Acta Mater. 58 (2010) 6282–6293.
[5] C. Xu, M.Y. Zheng, S.W. Xu, K. Wu, E.D. Wang, S. Kamado, et al., Mater. Sci. Eng. A 547 (2012) 93–98.
[6] Y. Kawamura, T. Kasahara, S. Izumi, M. Yamasaki, Scr. Mater. 55 (2006) 453–456.
[7] E.M. Padezhnova, E.V. Melnik, R. Milievskii, Russ. Metall. 4 (1982) 185–188.
[8] E. Abe, Y. Kawamura, K. Hayashi, A. Inoue, Acta Mater. 50 (2002) 3845–3857.
[9] T. Itoi, T. Seimiya, Y. Kawamura, M. Hirohashi, Scr. Mater. 51 (2004) 107–111.
[10] Y.M. Zhu, A.J. Morton, J.F. Nie, Acta Mater. 58 (2010) 2936–2947.
[11] Y.M. Zhu, A.J. Morton, J.F. Nie, Acta Mater. 60 (2012) 6562–6572.
[12] D. Egusa, E. Abe, Acta Mater. 60 (2012) 166–178.
[13] M. Matsuda, S. Ando, M. Nishida, Mater. Trans. 46 (2005) 361–364.
[14] A. Datta, U.V. Waghmare, U. Ramamurty, Acta Mater. 56 (2008) 2531–2539.
[15] K. Hagihara, N. Yokotani, Y. Umakoshi, Intermetallics 18 (2010) 267–276.
[16] K. Hagihara, Y. Sugino, Y. Fukusumi, Y. Umakoshi, T. Nakano, Mater. Trans. 52 (2011) 1096–1103.
[17] J.K. Kim, S. Sandlöbes, D. Raabe, Acta Mater. 82 (2015) 414–423.
[18] G. Garces, D.G. Morris, M.A. Muñoz-Morris, P. Perez, D. Tolnai, C. Mendis, Acta Mater. 94 (2015) 78–86.
[19] R.L. Xin, B. Song, K. Zeng, G. Huang, Q. Liu, Mater. Des. 34 (2012) 384–388.
[20] S.B. Yi, C.H.J. Davies, H.G. Brokmeier, R.E. Bolmaro, K.U. Kainer, J. Homeyer, Acta Mater. 54 (2006) 549–562.
[21] X.H. Shao, Z.Q. Yang, X.L. Ma, Philos. Mag. Lett. 94 (2014) 150–156.
[22] Y.B. Wang, B.Q. Li, M.L. Sui, S.X. Mao, Appl. Phys. Lett. 92 (2008) 011903.
[23] H. Somekawa, A. Singh, T. Mukai, Philos. Mag. Lett. 89 (2009) 2–10.
[24] X.H. Shao, Z.Q. Yang, X.L. Ma, Acta Mater. 5 (2010) 4760–4771.